

# Efficient Solvers for Nonlinear Time-Periodic Eddy Current Problems

F. Bachinger \*      U. Langer †      J. Schöberl ‡

August 17, 2004

## Abstract

This work deals with all aspects of the numerical simulation of nonlinear time-periodic eddy current problems, ranging from the description of the nonlinearity to an efficient solution procedure.

Due to the periodicity of the solution, we suggest a truncated Fourier series expansion, i.e. a so-called multiharmonic ansatz, instead of a costly time-stepping scheme. Linearization is done by a Newton iteration, where the preconditioning of the linearized problems is a special issue: Since the matrices are non-symmetric, we need a special adaptation of a multigrid preconditioner to our problem.

Eddy current problems comprise another difficulty that complicates the numerical simulation, namely the formation of extremely thin boundary layers. This challenge is handled by means of adaptive mesh refinement.

## 1 Introduction

In [4], we focussed mainly on theoretical issues that arise in the context of eddy current problems, whereas this paper concentrates on the aspects of their numerical simulation and on the construction of an efficient solver. Similar to the analytical paper [4], this work summarizes and extends the results that were achieved in [2].

For the numerical solution of general nonlinear eddy current problems with harmonic sources, there are some important features which one has to take into account:

- The magnetic reluctivity depends on the magnetic field in a nonlinear way.
- Since the source is periodical, the result will be periodical as well. However, due to the nonlinearity, the result will in general *not* be harmonic, but can be approximated by a Fourier series expansion.
- A truncated Fourier series expansion, i.e. a so-called multiharmonic ansatz, reduces the time-dependent equation to a system of equations in space for determining the Fourier coefficients. Finite element discretization of these equations yields a non-symmetric matrix. This fact complicates the issue of preconditioning.
- For a realistic setup, the magnetic field and the thereby generated eddy currents hardly penetrate into conducting materials and thus form an extremely thin boundary layer. Thus, the mesh for discretization has to meet special requirements.

---

\*Spezialforschungsbereich SFB F013, Johannes Kepler University Linz (since July 2004: VA Tech EBG Transformatoren (florian.bachinger@vatech.ebgtransformatoren.at)).

†Institute for Computational Mathematics, Johannes Kepler University Linz (ulanger@numa.uni-linz.ac.at).

‡START Project Y192, Institute for Computational Mathematics, Johannes Kepler University Linz (js@jku.at).

We remark that the simulation of electromagnetic devices in the frequency domain, i.e. by means of a harmonic or multiharmonic ansatz, has been pursued e.g. in [3, 7, 8, 18, 24]. The description of the nonlinearity is treated for example in [10, 19, 20].

This paper is structured as follows: After a brief review of some results of the theoretical work [4], we turn to the mentioned issues of the numerical simulation. First, we describe the nonlinear relation between the magnetic field and the induction in Section 3. Then, in Section 4 we comment on finite element methods for  $\mathbf{H}(\mathbf{curl}, \Omega)$ -problems and on multigrid preconditioners for such problems. Moreover, we explain the construction of our preconditioner for the non-symmetric problem. Section 5 is devoted to adaptive mesh refinement and nested iteration. Finally, in Section 6 we present and discuss our numerical results.

## 2 Problem Formulation

Eddy current problems can be described by system of partial differential equations

$$\sigma \frac{\partial \mathbf{u}}{\partial t} + \mathbf{curl} (\nu(|\mathbf{curl} \mathbf{u}|) \mathbf{curl} \mathbf{u}) = \mathbf{f} \quad (1)$$

in the computational domain  $\Omega$ , where  $\mathbf{f}$  denotes the sources,  $\sigma$  the conductivity and  $\nu$  the magnetic reluctivity;  $\mathbf{u}$  is the unknown vector potential. We remark that the reluctivity connects the induction  $\mathbf{B} = \mathbf{curl} \mathbf{u}$  and the magnetic field  $\mathbf{H}$  in the following way:

$$\mathbf{H} = \nu(|\mathbf{B}|)\mathbf{B}.$$

The problem (1) arises from the Maxwell equations (e.g. [13, 12, 15]). Under certain assumptions on the reluctivity  $\nu$ , which will be specified in Section 3, the eddy current equations (1) with appropriate boundary and initial conditions are uniquely solvable in a suitable class of divergence-free functions [4].

In many real life applications the source is an alternate current of the form  $\mathbf{f}(\mathbf{x}, t) = \hat{\mathbf{f}}(\mathbf{x}) \cdot \cos(\omega t)$ . We propose to take advantage of the resulting periodicity of the solution by a multiharmonic ansatz. This means, we suggest a truncated Fourier series expansion, what reduces the time-dependent problem to a system of equations in space. In [4] we have seen that the ansatz

$$\mathbf{u}(\mathbf{x}, t) \approx \sum_{k=0}^N [\mathbf{u}_k^c(\mathbf{x}) \cdot \cos(k\omega t) + \mathbf{u}_k^s(\mathbf{x}) \cdot \sin(k\omega t)], \quad (2)$$

for an odd number  $N$ , leads to the system

$$\mathbf{curl} \begin{pmatrix} \mathbf{H}_1^c(\mathbf{curl} \mathbf{u}) \\ \mathbf{H}_1^s(\mathbf{curl} \mathbf{u}) \\ \vdots \\ \mathbf{H}_N^c(\mathbf{curl} \mathbf{u}) \\ \mathbf{H}_N^s(\mathbf{curl} \mathbf{u}) \end{pmatrix} + \omega \sigma \underbrace{\begin{pmatrix} 0 & 1 & & & & \\ -1 & 0 & & & & \\ & & \ddots & & & \\ & & & 0 & N & \\ & & & -N & 0 & \end{pmatrix}}_{=: \mathbf{D}} \begin{pmatrix} \mathbf{u}_1^c \\ \mathbf{u}_1^s \\ \vdots \\ \mathbf{u}_N^c \\ \mathbf{u}_N^s \end{pmatrix} = \begin{pmatrix} \mathbf{f}_1^c \\ \mathbf{f}_1^s \\ \vdots \\ \mathbf{f}_N^c \\ \mathbf{f}_N^s \end{pmatrix}, \quad (3)$$

where the even harmonics  $\mathbf{u}_{2k}^c, \mathbf{u}_{2k}^s$  are a priori known to be zero. By the vector  $(\mathbf{H}_1^c, \mathbf{H}_1^s, \mathbf{H}_3^c, \mathbf{H}_3^s, \dots, \mathbf{H}_N^c, \mathbf{H}_N^s)^T$  in (3) we denote the Fourier coefficients of the magnetic field  $\mathbf{H} = \mathbf{H}(\mathbf{curl} \mathbf{u})$ . Introducing the abbreviation  $\mathbf{u} = (\mathbf{u}_1^c, \mathbf{u}_1^s, \mathbf{u}_3^c, \mathbf{u}_3^s, \dots, \mathbf{u}_N^c, \mathbf{u}_N^s)^T$  and similarly for  $\mathbf{f}$  and  $\mathbf{H}$ , we can rewrite (3) as

$$\mathbf{curl} \mathbf{H}(\mathbf{curl} \mathbf{u}) + \omega \sigma \mathbf{D} \mathbf{u} = \mathbf{f}. \quad (4)$$

We could show in [4] that the error between the exact solution and the truncated Fourier series (2) is of the order  $N^{-1}$ , provided that  $\mathbf{u}$  is twice differentiable in time. Thus the multiharmonic ansatz is well justified.

The rest of this paper is dedicated to the numerical solution of equation (4) in some bounded domain  $\Omega$  together with homogeneous Dirichlet boundary conditions  $\mathbf{u} \times \mathbf{n} = 0$  on  $\partial\Omega$ .

As mentioned previously, unique solvability can only be guaranteed among the divergence-free functions. However, by assuming a strictly positive conductivity  $\sigma$  in the entire region  $\Omega$ , we can ensure unique solvability in the whole space  $\mathbf{H}(\mathbf{curl}, \Omega)$ . Since in general the computational domain can consist of both non-conducting and conducting material, we regularize the problem by setting

$$\sigma_\epsilon(\mathbf{x}) = \max\{\sigma(\mathbf{x}), \epsilon\},$$

for some small  $\epsilon > 0$ . We mention that this regularization was rigorously justified in [4].

### 3 The Handling of the $\mathbf{B}$ - $\mathbf{H}$ -Curve

One of the major tasks that we have to deal with in eddy current problems is the nonlinear relation between  $\mathbf{B}$  and  $\mathbf{H}$ . In practical applications, this relation is given by a set of measured data points that provide the connection between  $|\mathbf{B}|$  and  $|\mathbf{H}|$  (cf. Figure 1). These data points are approximated [19, 20] or interpolated [10] (e.g. by splines) to provide a continuous  $\mathbf{B}$ - $\mathbf{H}$ -curve  $|\mathbf{B}| = b(|\mathbf{H}|)$  with certain properties. This curve is supposed to be strictly monotone.

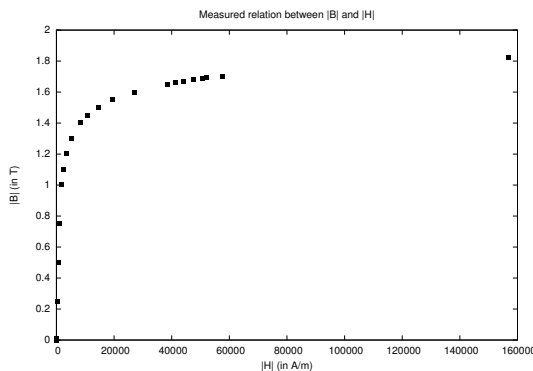


Figure 1: Example of measured data points for a  $\mathbf{B}$ - $\mathbf{H}$ -curve.<sup>1</sup>

Obviously,  $\nu$  can easily be calculated once you know the relation  $|\mathbf{B}| = b(|\mathbf{H}|)$ :

$$\nu(s) = \frac{b^{-1}(s)}{s}. \quad (5)$$

Due to the physical background the function  $\nu : \mathbb{R}_0^+ \rightarrow \mathbb{R}^+$  fulfills certain properties:

$$0 < \underline{\nu} \leq \nu(s) \leq \nu_0, \quad \forall s \in \mathbb{R}_0^+, \quad \text{and} \quad \lim_{s \rightarrow \infty} \nu(s) = \nu_0, \quad (6)$$

where  $\nu_0$  is the reluctivity in vacuum (cf. [20]).

Note that, since the  $\mathbf{B}$ - $\mathbf{H}$ -curve is strictly monotone, also its inverse, i.e. the function  $s \mapsto \nu(s) \cdot s$ , is strictly monotone. This fact was important in [4] for proving unique solvability of the nonlinear boundary value problem. Moreover, the function  $s \mapsto \nu(s) \cdot s$  is Lipschitz continuous (cf. [19]). Furthermore, it is reasonable to assume that this function is continuously differentiable.

In this paper we use the function shown in Figure 2 that was approximated from measured data for iron according to [20]. As the figure clearly shows, the nonlinearity is strongest at a magnetic flux density of approximately 1.5 Tesla. For small and very large inductions  $|\mathbf{B}|$ , the reluctivity  $\nu(|\mathbf{B}|)$  is almost constant.

<sup>1</sup>The magnetic field intensity  $|\mathbf{H}|$  is measured in Ampere/meter, the flux density  $|\mathbf{B}|$  in Tesla. Data is a courtesy of Manfred Kaltenbacher, Department of Sensor Technology, University of Erlangen.

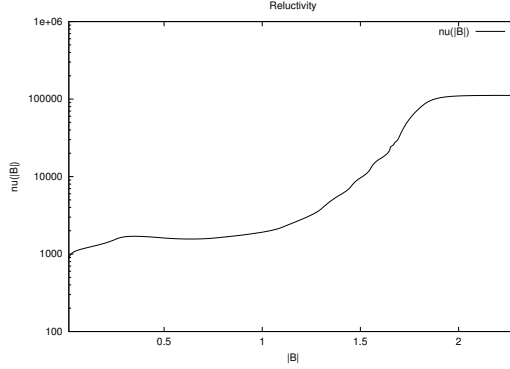


Figure 2: Reluctivity  $\nu(|\mathbf{B}|)$  for a ferromagnetic material.

## 4 Linearization, Discretization and Preconditioning

For the numerical solution of the nonlinear problem (4), we rewrite it in weak formulation. For this sake, we define the spaces

$$\begin{aligned} \mathbf{V} &:= \{\mathbf{v} \in \mathbf{L}_2(\Omega) : \mathbf{curl} \mathbf{v} \in \mathbf{L}_2(\Omega)\} = \mathbf{H}(\mathbf{curl}, \Omega), \\ \mathbf{V}_0 &:= \{\mathbf{v} \in \mathbf{V} : \mathbf{v} \times \mathbf{n} = 0 \text{ on } \partial\Omega\}. \end{aligned}$$

Thus, (4) transforms to the variational problem

$$\langle A(\mathbf{u}), \mathbf{v} \rangle + \langle M\mathbf{u}, \mathbf{v} \rangle = (\mathbf{f}, \mathbf{v}), \quad \forall \mathbf{v} \in \mathbf{V}_0^{N+1}, \quad (7)$$

where the operators  $A$  and  $M$  are defined as follows:

$$\langle A(\mathbf{u}), \mathbf{v} \rangle := \int_{\Omega} \mathbf{H}(\mathbf{curl} \mathbf{u}) \cdot \mathbf{curl} \mathbf{v} \, dx, \quad \forall \mathbf{u}, \mathbf{v} \in \mathbf{V}_0^{N+1}, \quad (8)$$

$$\langle M\mathbf{u}, \mathbf{v} \rangle := \omega \int_{\Omega} \sigma_{\epsilon} \mathbf{D}\mathbf{u} \cdot \mathbf{v} \, dx, \quad \forall \mathbf{u}, \mathbf{v} \in \mathbf{V}_0^{N+1}. \quad (9)$$

Here an element  $\mathbf{v} \in \mathbf{V}_0^{N+1}$  is a vector of Fourier coefficients  $\mathbf{v} = (\mathbf{v}_1^c, \mathbf{v}_1^s, \mathbf{v}_3^c, \mathbf{v}_3^s, \dots, \mathbf{v}_N^c, \mathbf{v}_N^s)^T$ . Note that  $N$  means the (odd) number of harmonics. The superscripts  $c$  and  $s$  indicate the coefficient of cosine and sine, respectively.<sup>2</sup>  $\mathbf{D}$  is the matrix defined in (3), i.e.

$$\mathbf{D} = \begin{pmatrix} 0 & 1 & & & & & \\ -1 & 0 & & & & & \\ & & \ddots & & & & \\ & & & 0 & N & & \\ & & & -N & 0 & & \end{pmatrix}.$$

$\mathbf{H}(\mathbf{curl} \mathbf{u})$  denotes the Fourier coefficients of the magnetic field  $\mathbf{H}(\mathbf{curl} \mathbf{u}(t))$ .

In order to keep notation simple, we denote by  $\mathbf{u}$  the vector of Fourier coefficients, and by  $\mathbf{u}(t)$  the multiharmonic function that is determined by these coefficients. Thus we have, for example,

$$\mathbf{curl} \mathbf{u}(t) = \sum_{l=1}^N (\mathbf{curl} \mathbf{u}_l^c \cos(l\omega t) + \mathbf{curl} \mathbf{u}_l^s \sin(l\omega t)).$$

<sup>2</sup>We emphasize again that the even harmonics need not be considered, cf. [4].

Additionally, we mention that the coefficients  $\mathbf{H}(\mathbf{curl} \mathbf{u})$  can be calculated by Fourier transformation in the following way:

$$\mathbf{H}_k^c(\mathbf{curl} \mathbf{u}) = \frac{2}{T} \int_0^T \nu(|\mathbf{curl} \mathbf{u}(t)|) \cdot \mathbf{curl} \mathbf{u}(t) \cdot \cos(k\omega t) dt, \quad (10)$$

$$\mathbf{H}_k^s(\mathbf{curl} \mathbf{u}) = \frac{2}{T} \int_0^T \nu(|\mathbf{curl} \mathbf{u}(t)|) \cdot \mathbf{curl} \mathbf{u}(t) \cdot \sin(k\omega t) dt. \quad (11)$$

#### 4.1 Newton Iteration

Due to its superlinear (or even quadratic) convergence, Newton's method seems to be a good choice for the linearization of the nonlinear multiharmonic problem (7). In order to implement this method, we have to calculate the Fréchet derivative of the operators  $A$  and  $M$ , which are defined in (8) and (9), respectively.

Since  $M$  is a linear operator, its derivative is just  $M$  again. The Fréchet derivative of the nonlinear operator  $A$  applied to some  $\mathbf{w} \in \mathbf{V}_0^{N+1}$  can obviously be written as

$$\langle A'(\mathbf{u})\mathbf{w}, \mathbf{v} \rangle = \int_{\Omega} \left[ \frac{\partial \mathbf{H}}{\partial \mathbf{B}}(\mathbf{curl} \mathbf{u}) \mathbf{curl} \mathbf{w} \right] \cdot \mathbf{curl} \mathbf{v} dx. \quad (12)$$

It remains to clarify what we mean by the derivative  $\frac{\partial \mathbf{H}}{\partial \mathbf{B}}$ :

$$\begin{aligned} \frac{\partial \mathbf{H}_k^c}{\partial \mathbf{B}_i^c}(\mathbf{B}) &= \frac{\partial}{\partial \mathbf{B}_i^c} \left( \frac{2}{T} \int_0^T \underbrace{\nu(|\mathbf{B}(t)|)\mathbf{B}(t)}_{=\mathbf{H}(\mathbf{B}(t))} \cos(k\omega t) dt \right) = \\ &= \frac{2}{T} \int_0^T \frac{\partial \mathbf{H}(\mathbf{B}(t))}{\partial \mathbf{B}(t)} \cos(l\omega t) \cos(k\omega t) dt = \end{aligned} \quad (13a)$$

$$= \frac{2}{T} \int_0^T \left[ \nu'(|\mathbf{B}(t)|) \frac{\mathbf{B}(t)\mathbf{B}(t)^T}{|\mathbf{B}(t)|} + \nu(|\mathbf{B}(t)|)\mathbf{I} \right] \cos(l\omega t) \cos(k\omega t) dt, \quad (13b)$$

with the  $3 \times 3$  - identity matrix  $\mathbf{I}$ . It should be mentioned that  $\mathbf{B}(t)\mathbf{B}(t)^T$  is a  $3 \times 3$  - matrix of rank 1. For points in time with  $\mathbf{B}(t) = 0$ , the derivative  $\frac{\partial \mathbf{H}(\mathbf{B}(t))}{\partial \mathbf{B}(t)}$  in (13a) actually reduces to

$$\lim_{|\mathbf{B}| \rightarrow 0} \frac{\mathbf{H}(|\mathbf{B}|) - \mathbf{H}(0)}{|\mathbf{B}| - 0} = \lim_{|\mathbf{B}| \rightarrow 0} \frac{\mathbf{H}(|\mathbf{B}|)}{|\mathbf{B}|} = \nu(0)\mathbf{I}.$$

So the integrand in the explicit calculation of the derivative (13b) should be understood as  $\nu(0)\mathbf{I}$  for  $\mathbf{B}(t) = 0$ .

Similarly, the other derivatives  $\frac{\partial \mathbf{H}_k^c}{\partial \mathbf{B}_i^s}$ ,  $\frac{\partial \mathbf{H}_k^s}{\partial \mathbf{B}_i^c}$  and  $\frac{\partial \mathbf{H}_k^s}{\partial \mathbf{B}_i^s}$  can be calculated. Note that all of them exist, since the  $\mathbf{B}$ - $\mathbf{H}$ -curve was assumed to be differentiable.

*Example.* For better understanding what the complete matrix  $\frac{\partial \mathbf{H}}{\partial \mathbf{B}}$  in (12) looks like, we quote the example of one harmonic. In this case we have

$$\mathbf{u} = (\mathbf{u}^c, \mathbf{u}^s)^T, \quad \mathbf{H} = (\mathbf{H}^c, \mathbf{H}^s)^T.$$

Then the derivative is the matrix

$$\frac{\partial \mathbf{H}}{\partial \mathbf{B}}(\mathbf{curl} \mathbf{u}) = \begin{pmatrix} \frac{\partial \mathbf{H}^c}{\partial \mathbf{B}^c}(\mathbf{curl} \mathbf{u}) & \frac{\partial \mathbf{H}^c}{\partial \mathbf{B}^s}(\mathbf{curl} \mathbf{u}) \\ \frac{\partial \mathbf{H}^s}{\partial \mathbf{B}^c}(\mathbf{curl} \mathbf{u}) & \frac{\partial \mathbf{H}^s}{\partial \mathbf{B}^s}(\mathbf{curl} \mathbf{u}) \end{pmatrix},$$

with each of its entries being calculated as derived in (13).

## 4.2 A Multigrid Preconditioner for a Non-Symmetric System

We discretize the system of PDEs (4) by means of the finite element method. Since we deal with a problem in the space  $\mathbf{V}$ , the preferable choice are Nédélec elements [16, 17], which are conforming in this space, see e.g. [15].

It is well known that the system matrices arising from the finite element discretization of problems like (4) are ill-conditioned. The condition number rapidly grows for decreasing mesh size. Consequently, preconditioning is required in order to achieve fast iterative solution of the linear systems.

Multigrid has proven to be among the most efficient preconditioners for discretized PDEs. Their efficiency is based on the interaction between *smoothing* and *coarse grid correction*. We emphasize that for problems in the space  $\mathbf{V}$  a special smoother is required for obtaining a fast convergence of the multigrid iteration. Arnold, Falk and Winther suggest additive and multiplicative Schwarz smoothers based on vertex patches in [1]. Alternatively, Hiptmair proposed a smoother with additional relaxation sweeps in the potential space in [11].

Equipped with this knowledge about an appropriate smoother, the construction of a multigrid preconditioner is not difficult. However, it is not obvious how to precondition the non-symmetric problem that we are concerned with.

For the sake of simplicity, we consider only the (perturbed) linear harmonic problem for the moment. The finite element discretization leads to the system

$$\underbrace{\begin{pmatrix} A & M \\ -M & A \end{pmatrix}}_{=:K} \begin{pmatrix} u^c \\ u^s \end{pmatrix} = \begin{pmatrix} f^c \\ f^s \end{pmatrix}. \quad (14)$$

Here the matrix  $A = A_h$  is the discretization of the singular operator

$$\langle A\mathbf{u}, \mathbf{v} \rangle = \int_{\Omega} \nu \operatorname{curl} \mathbf{v}^T \operatorname{curl} \mathbf{u} \, d\mathbf{x},$$

and  $M = M_h$  results from

$$\langle M\mathbf{u}, \mathbf{v} \rangle = \int_{\Omega} \omega \sigma_{\epsilon} \mathbf{v}^T \mathbf{u} \, d\mathbf{x},$$

where in (14) as well as in the sequel we omit the subscript  $h$ . By  $u^c \in \mathbb{R}^n$  we mean the discretization of  $\mathbf{u}^c$ , and analogously for  $u^s$ ,  $f^c$  and  $f^s$ .

Since multigrid theory is well understood for symmetric problems, we apply a multigrid iteration to an artificial symmetric problem and by this means construct a preconditioner for the non-symmetric matrix  $K$  as defined in (14).

More precisely, we propose to choose the preconditioner  $C$  in the form

$$C^{-1} = \frac{1}{2} \begin{pmatrix} (A+M)^{-1} & 0 \\ 0 & (A+M)^{-1} \end{pmatrix} \begin{pmatrix} I & I \\ I & -I \end{pmatrix}, \quad (15)$$

where the inverse of  $A+M$  is approximated by a symmetric multigrid iteration.

Numerical results show – also in the case of approximated inverse – the fast convergence of Krylov space iteration methods, independently of mesh size and parameters (see Table 1). Moreover, we can prove the following result on a condition number bound by purely algebraic arguments:

**Lemma 1.** *With  $K \in \mathbb{R}^{2n \times 2n}$  defined as in (14) and  $C^{-1}$  as in (15), we have the estimate*

$$\kappa(C^{-1}K) \leq 2,$$

if we define  $\kappa(A) = \|A\| \cdot \|A^{-1}\|$  and choose the vector norm in  $\mathbb{R}^{2n}$  by  $\|u\|_{A+M} = \|(u^c, u^s)^T\|_{A+M} := [((A+M)u^c, u^c) + ((A+M)u^s, u^s)]^{\frac{1}{2}}$ .

*Proof.* In the following, we refer to  $(u^c, u^s)^T \in \mathbb{R}^{2n}$  by  $u$ . We introduce – both for  $v \in \mathbb{R}^n$  and  $v \in \mathbb{R}^{2n}$  – the abbreviation  $(v, v)_1 := (v, v)_{A+M} = ((A+M)v, v)$ , where  $(\cdot, \cdot)$  denotes the Euclidean scalar product. The same notation is used for the norm.

The condition number is calculated by

$$\kappa(C^{-1}K) = \|C^{-1}K\|_1 \cdot \|(C^{-1}K)^{-1}\|_1. \quad (16)$$

The first factor equals

$$\|C^{-1}K\|_1 = \sup_u \frac{\|C^{-1}Ku\|_1}{\|u\|_1} = \sup_{u,v} \frac{(C^{-1}Ku, v)_1}{\|u\|_1 \|v\|_1},$$

and we have

$$(C^{-1}Ku, v)_1 = ((A+M)C^{-1}Ku, v) = (Bu, v), \quad (17)$$

with the matrix

$$B = \frac{1}{2} \begin{pmatrix} A-M & A+M \\ A+M & M-A \end{pmatrix}.$$

Consequently, (17) is bounded from above by  $\|u\|_1 \cdot \|v\|_1$ , since

$$(Bu, v) = \frac{1}{2} [(A-M)u^c, v^c] + (u^s, v^c)_1 + (u^c, v^s)_1 + ((M-A)u^s, v^s), \quad (18)$$

and because an elementary discussion shows

$$\begin{aligned} (Bu, v) &\leq \frac{1}{2} [\|u^c\|_1 \|v^c\|_1 + \|u^s\|_1 \|v^c\|_1 + \|u^c\|_1 \|v^s\|_1 + \|u^s\|_1 \|v^s\|_1] \\ &\leq \left[ \|u^c\|_1^2 + \|u^s\|_1^2 \right]^{\frac{1}{2}} \cdot \left[ \|v^c\|_1^2 + \|v^s\|_1^2 \right]^{\frac{1}{2}} = \|u\|_1 \cdot \|v\|_1. \end{aligned}$$

Thus, we have  $\|C^{-1}K\|_1 \leq 1$ . It remains to analyze the second term in (16):

$$\|(C^{-1}K)^{-1}\|_1 = \sup_u \frac{\|u\|_1}{\|C^{-1}Ku\|_1}, \quad (19)$$

and

$$\|C^{-1}Ku\|_1 = \sup_v \frac{(C^{-1}Ku, v)_1}{\|v\|_1} = \sup_v \frac{(Bu, v)}{\|v\|_1} \geq \frac{(B \begin{pmatrix} u^c \\ u^s \end{pmatrix}, \begin{pmatrix} u^c \\ u^c \end{pmatrix})}{\|u\|_1}.$$

Simple calculations yield  $(B \begin{pmatrix} u^c \\ u^s \end{pmatrix}, \begin{pmatrix} u^c \\ u^c \end{pmatrix}) = \frac{1}{2} \|u\|_1^2$ , and consequently  $\|C^{-1}Ku\|_1 \leq 2$ . Combining these bounds, we arrive at the final estimate

$$\kappa(C^{-1}K) = \|C^{-1}K\|_1 \cdot \|(C^{-1}K)^{-1}\|_1 \leq 1 \cdot 2 = 2.$$

□

Let us now demonstrate the quality of the preconditioner (15) for the solution of the system

$$\text{Find } u = \begin{pmatrix} u^c \\ u^s \end{pmatrix} \in \mathbb{R}^{2n} : \quad Ku = \begin{pmatrix} A & M \\ -M & A \end{pmatrix} \begin{pmatrix} u^c \\ u^s \end{pmatrix} = \begin{pmatrix} f^c \\ f^s \end{pmatrix}, \quad (14)$$

by numerical computations. We solve the non-symmetric linear system (14) by the quasi-minimal residual method (QMR) [6] with the preconditioner (15). Table 1 presents the number of steps needed to reach a relative accuracy  $10^{-6}$  for different parameter settings and dimensions of the finite element space.

All these examples are test cases of the shielding problem that is described in Section 6. The parameter  $\sigma_{Fe}$  denotes the conductivity in the iron plate (measured in  $\frac{\text{S}}{\text{m}}$ ),  $\epsilon$  refers to the regularization parameter – we use the conductivity  $\epsilon \cdot \sigma_{Fe}$  for the non-conducting regions – and  $\omega$  means the angular frequency  $2\pi f$ . In all these cases, the reluctivity  $\nu$  is set to  $\nu_{Fe} = \frac{1}{\mu_0 \mu_{Fe}} = \frac{1}{4\pi \cdot 10^{-4}} \approx 8 \cdot 10^2 \frac{\text{m}}{\text{H}}$  in the iron domain and to  $\nu_0 = \frac{1}{\mu_0} = \frac{1}{4\pi \cdot 10^{-7}} \approx 8 \cdot 10^5 \frac{\text{m}}{\text{H}}$  in the coil and the surrounding air.

As can be seen in Table 1, the number of QMR iterations is independent of both dimension of the FE-space and choices of the parameters.

Parameters	$n$	1627	4942	19407	44306	68363	105225
$\sigma_{Fe} = 10^4, \epsilon = 10^{-7}, \omega = 10^2\pi$		10	10	12	12	12	12
$\sigma_{Fe} = 10^5, \epsilon = 10^{-7}, \omega = 10^2\pi$		14	11	12	12	13	13
$\sigma_{Fe} = 10^5, \epsilon = 10^{-7}, \omega = 10^3\pi$		16	14	14	14	14	14
$\sigma_{Fe} = 10^5, \epsilon = 10^{-7}, \omega = 10^4\pi$		14	14	14	14	14	16
$\sigma_{Fe} = 10^6, \epsilon = 10^{-7}, \omega = 10^3\pi$		14	14	14	14	14	16
$\sigma_{Fe} = 10^6, \epsilon = 10^{-9}, \omega = 10^3\pi$		14	14	14	14	16	16
$\sigma_{Fe} = 10^6, \epsilon = 10^{-11}, \omega = 10^3\pi$		15	15	14	14	14	14

Table 1: Number of QMR iterations for the solution of the linear problem with respect to different dimensions and parameters.

## 5 Adaptive Refinement and Nested Iteration

### 5.1 A Note on the Penetration Depth

A remarkable feature of eddy current problems is the fact that both magnetic field and eddy currents scarcely penetrate into conducting materials but form a layer of strong induction at the boundary. The skin depth depends on the permeability and the conductivity of the material as well as on the frequency of the source current. This phenomenon is described by the following formula for the penetration depth, which gives the depth where the magnetic field has declined to an  $e^{-1}$ -th of its original value, i.e. by more than 60 % (see e.g. [13], page 151):

$$\delta = \sqrt{\frac{2}{\omega\mu\sigma}}. \quad (20)$$

For usual ferromagnetic materials we are confronted with conductivities of approximately  $\sigma \approx 10^6 \frac{\text{S}}{\text{m}}$  and – at least for small inductions, where  $\nu(|\mathbf{B}|) = \mu^{-1}(|\mathbf{H}|) \approx \text{const}$  – permeabilities  $\mu \approx 4\pi \cdot 10^{-4} \frac{\text{H}}{\text{m}}$ . Already in the case of a frequency  $f = 50 \text{ Hz}$ , i.e.  $\omega = 100\pi$ , this results in a penetration depth of  $\delta \approx 0.00225 \text{ m}$ .

This means that even for low frequencies we can observe the formation of a skin at the boundaries of conducting materials. The situation is even more dramatic for the problem of eddy current welding, where we usually are concerned with a source current of 200 kHz. In this case a skin of approximately  $\delta \approx 0.0000356 \text{ meters}$  occurs, or even worse, since in the realistic setup we have a conductivity of  $\sigma = 9.3 \cdot 10^6$  that leads to  $\delta \approx 1.17 \cdot 10^{-5} \text{ m}$ .

Therefore, it is obviously necessary to mesh this skin adequately. This would result in a substantial number of unknowns. However, we are able to keep their amount at an acceptable level by adaptive refinement of this small layer.

### 5.2 Remarks Concerning Implementation

The mesh for discretization is generated by the automatic mesh generator NETGEN [22] that has been developed at the University of Linz. The whole solver is implemented as a module of the finite element package NGSolve [21] (developed at the University of Linz as well), see also [14].

As we have seen in Section 4, in each step of the Newton iteration a linear problem with system matrix  $A'(\mathbf{u}) + M$  has to be solved.  $A'(\mathbf{u})$  consists of entries

$$\frac{\partial \mathbf{H}_k^c}{\partial \mathbf{B}_l^c}(\mathbf{curl} \mathbf{u}) = \frac{2}{T} \int_0^T \frac{\partial \mathbf{H}(\mathbf{curl} \mathbf{u}(t))}{\partial \mathbf{B}(t)} \cos(l\omega t) \cos(k\omega t) dt,$$



that have to be calculated for the assembly of the linearized matrix. We evaluate these integrals by numerical integration, although a faster integration based on fast Fourier transformation could be envisaged. This, however, seems to be of secondary importance, since the solution of the linear systems is much more time consuming than their assembly.

The linearized problem in each Newton step is solved by a QMR iteration [6] which is preconditioned by a block diagonal preconditioner of the following form:

$$C = \begin{pmatrix} C_1 & & & \\ & C_3 & & \\ & & \ddots & \\ & & & C_N \end{pmatrix} \quad \text{with } C_k^{-1} = \frac{1}{2} \begin{pmatrix} (A(\bar{\nu}) + kM)^{-1} & 0 \\ 0 & (A(\bar{\nu}) + kM)^{-1} \end{pmatrix} \begin{pmatrix} I & -I \\ I & I \end{pmatrix}.$$

The blocks  $C_i$  are similar to (15) for one harmonic, where we use a time-averaged reluctivity  $\bar{\nu}$  and the exact inverses are replaced by one symmetric multigrid cycle.

Table 2 confirms the quality of our preconditioner even for strong influences of the nonlinearity. In the table we show results of computations for the shielding problem (cf. Section 6). We depict the number of QMR steps needed to reach a relative accuracy of  $10^{-6}$ . Even when  $\nu'$  reaches large values, i.e. for  $|\mathbf{B}| \approx 1.5$  (cf. Figure 2), we observe fairly good convergence properties of the QMR iteration.

Computations were done on two different meshes and for various strength of the source current, i.e. for different induction in the solution, which is depicted in the second column.

The third column in the table shows the iterative solution of the linear problem, whereas the subsequent columns display the Newton iteration and the number of QMR steps for the solution of the linearized problems.

$n$	$\max  \mathbf{B} $	QMR-Steps in the Newton iteration							
44306	0.3 T	14	18	16					
	1.38 T	14	21	19	17	17			
	1.61 T	14	65	34	33	32	31	31	
	1.76 T	14	125	48	54	49	47	40	38
105225	0.39 T	14	18	18					
	1.33 T	14	19	19	17				
	1.67 T	14	42	28	28	27	27		
	1.74 T	14	86	47	45	38	40	40	35

Table 2: QMR steps for the solution of the linearized problems in the Newton iteration.

### 5.3 Nested Iteration

For the general solution procedure, we apply a so-called *nested iteration* (cf. [9]). This means that we start on the coarsest grid and calculate an approximate solution  $u_0$  of the nonlinear problem on this level. Then the mesh is refined adaptively and the prolongation of  $u_0$  to the next level yields a good initial guess for  $u_1$ , the approximate solution on level 1. This algorithm is continued until a sufficiently fine level is reached.

In order to reach good approximation with a comparatively small number of unknowns, an adaptive refinement procedure on the basis of local error estimators is essential. In this work, we make use of a Zinkiewicz-Zhu error estimator [25, 26]. In this context we additionally refer to other works on a-posteriori error estimation and adaptive refinement, e.g. [5, 23].

Bearing in mind that the solutions on the coarser grids are needed only for error estimates and as initial guesses for the Newton iteration on the finer grid, different strategies of adaptive refinement

can be considered: inexact solution on each of the coarser levels, while the fine level is solved more accurately, for example, or a consistent increase in accuracy after each refinement step. Another idea is to solve the linearized systems less exactly, since for achieving a Newton accuracy of  $10^{-3}$ , for instance, it is unnecessary to push the QMR iteration to a relative accuracy of  $10^{-6}$ .

In the following, we compare the strategies of nested iteration that are described in Table 3, where, when we proceed according to (S0), we do not use the prolonged solution of the coarser level as initial guess for the Newton iteration, but the solution of the linear problem. So (S0) is actually not a nested iteration.

Strategy:	Newton accuracy on level $l$	QMR accuracy on level $l$
(S0) non-nested	$\epsilon_l^N = \epsilon^N = 10^{-8}$	$\epsilon_l^Q = \epsilon^Q = 10^{-6}$
(S1)	$\epsilon_l^N = \epsilon^N = 10^{-8}$	$\epsilon_l^Q = \epsilon^Q = 10^{-6}$
(S1')	$\epsilon_l^N = \epsilon^N = 10^{-8}$	$\epsilon_l^Q = \epsilon^Q = 10^{-4}$
(S2)	$\epsilon_l^N = 10^{-2} \cdot 10^{-l}$ , for $l < l_{\max}$ , $\epsilon_{l_{\max}}^N = 10^{-8}$	$\epsilon_l^Q = \max\{\epsilon_l^N, 10^{-6}\}$
(S3)	$\epsilon_l^N = 10^{-3}$ , for $l < l_{\max}$ , $\epsilon_{l_{\max}}^N = 10^{-8}$	$\epsilon_l^Q = \max\{\epsilon_l^N, 10^{-6}\}$
(S4)	$\epsilon_0^N = 10^{-6}$ , $\epsilon_l^N = 10^{-3}$ , for $0 < l < l_{\max}$ , $\epsilon_{l_{\max}}^N = 10^{-8}$	$\epsilon_l^Q = \max\{\epsilon_l^N, 10^{-6}\}$

Table 3: Different strategies of nested iteration.

Table 4 compares the accumulated number of QMR iterations on each level together with the time needed for the solution. Again, we consider the shielding problem (cf. Section 6), with a current of  $5 \cdot 10^5$  A in the coil, i.e. we observe a maximal induction  $|\mathbf{B}| \approx 1.83$  T in the solution. Although this table presents results for one harmonic, we emphasize that we observe analogous results for a different number of modes. We remark that the computations shown in Table 4 are achieved by the lowest order Nédélec edge discretization of the first kind. Anyhow, even though the results for higher order basis functions differ slightly from those in the table, the general superiority of inexact solution on coarser levels is exactly the same.

For Table 4, we begin with a coarse grid with  $n = 4942$  degrees of freedom, and then adaptively refine the mesh. The different strategies of nested iteration yield comparable sequences of grids – strategies (S0), (S1), (S1'), (S3) and (S4) yield  $n = 31255$  on level 1,  $n = 78665$  on level 2,  $n = 91851$  on level 3 and finally with 92211 degrees of freedom on the finest mesh, level 4, whereas (S2) results in the sequence  $n = 31264 / 78631 / 91823 / 92013$ .

The table impressively demonstrates the superiority of nested iterations over the non-nested strategy (S0), as well as the preeminence of procedures that solve less accurately on the coarser levels. A comparison of (S3), where we solve fairly inexactly on all the coarse levels, with the approach (S4) displays that more effort on the first comparably coarse grid pays off in the end.

## 6 Numerical Results

In this section, we present the results of our computations for two real-life problems, which are depicted in Figure 3. For both problems, we assume a given current in the coil and calculate the magnetic field and eddy currents in the conducting regions and some surrounding air.

<sup>3</sup>The computations were done on an AMD™ Athlon™ CPU with 1800 MHz.

Strategy $n =$	Level 0 4942	Level 1 31255	Level 2 78665	Level 3 91851	Level 4 92211	Total Time
(S0) non-nested	46 0.24 min	134 5.57 min	630 64.02 min	638 110.33 min	619 151.4 min	331.6 min
(S1)	46 0.24 min	131 5.77 min	594 60.87 min	356 62.13 min	166 41.14 min	170.1 min
(S1')	34 0.2 min	93 4.74 min	442 46.89 min	235 42.72 min	105 26.52 min	121.1 min
(S2)	4 0.02 min	44 2.8 min	349 37.16 min	236 42.39 min	100 24.84 min	107.2 min
(S3)	17 0.1 min	44 2.79 min	240 26.34 min	90 16.78 min	174 43.04 min	89.1 min
(S4)	30 0.15 min	44 2.78 min	235 25.6 min	84 15.83 min	172 41.93 min	86.3 min

Table 4: Total number of QMR steps per level and solution time for various strategies of nested iteration.<sup>3</sup>

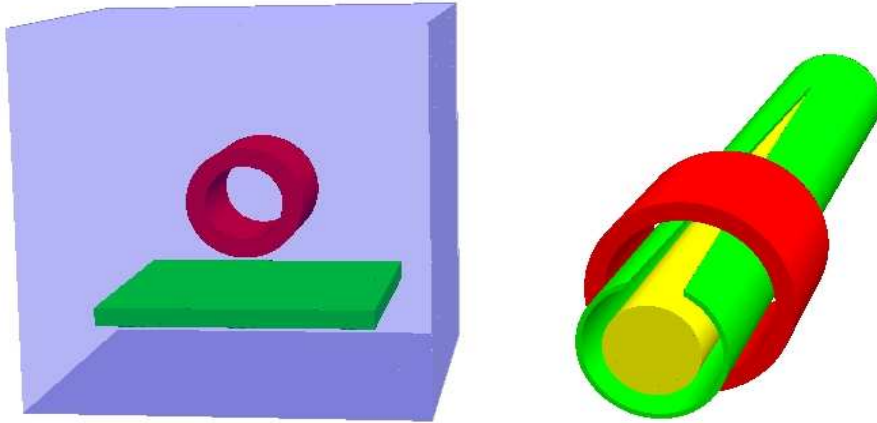


Figure 3: Geometries of a shielding (left) and a welding problem (right).

For the shielding problem, we use the following parameter setting: conductivity of the iron plate  $\sigma_{Fe} = 10^6 \frac{S}{m}$ , in the rest of the domain  $\sigma = \epsilon \cdot \sigma_{Fe}$  with  $\epsilon = 10^{-9}$ , frequency  $f = 50$  Hz. With eddy current welding, we face a frequency of  $f = 200$  kHz and a conductivity of  $\sigma_{Fe} = 9.3 \cdot 10^6 \frac{S}{m}$  in the slitted tube.

## 6.1 Number of Harmonics

By [4] we know that the error between the exact solution and the truncated Fourier series

$$\sum_{k=0}^N [\mathbf{u}_k^c(\mathbf{x}) \cdot \cos(k\omega t) + \mathbf{u}_k^s(\mathbf{x}) \cdot \sin(k\omega t)],$$

is at most of the order  $N^{-1}$ . For smooth solutions, one might expect faster convergence. In fact, experiments showed that this estimate is in general too pessimistic. Figure 4 illustrates the fast convergence for increasing  $N$  for the example of the shielding problem. The figure depicts the total eddy current density in the conducting region for computations with various numbers of harmonics.

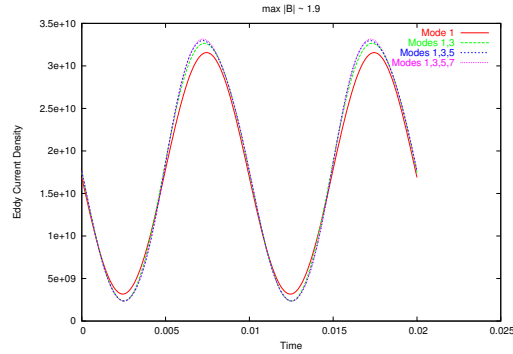
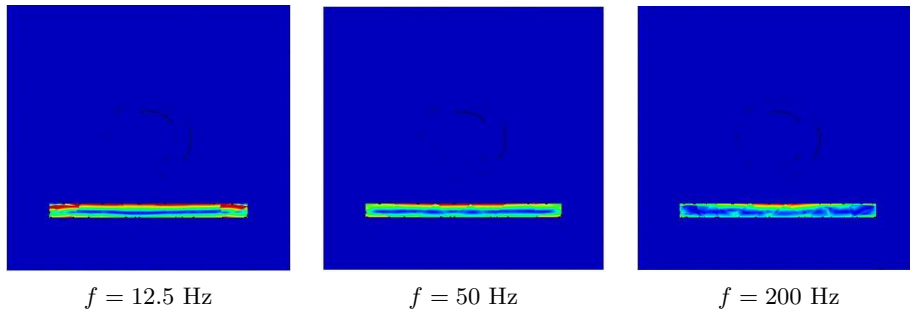


Figure 4: Eddy current density for different numbers of harmonics.

## 6.2 Results

Finally, we present some results for both the shielding and the welding problem: Figures 5 and 6 plot the absolute value of the eddy currents in a clipping plane.

In addition to the general result with strong currents in a thin layer, Figure 5 depicts the influence of the frequency on the skin depth. According to formula (20), quadrupling the frequency should shrink the layer to  $\frac{1}{2}$  of the original size. This effect can be observed quite conspicuously in Figure 5.

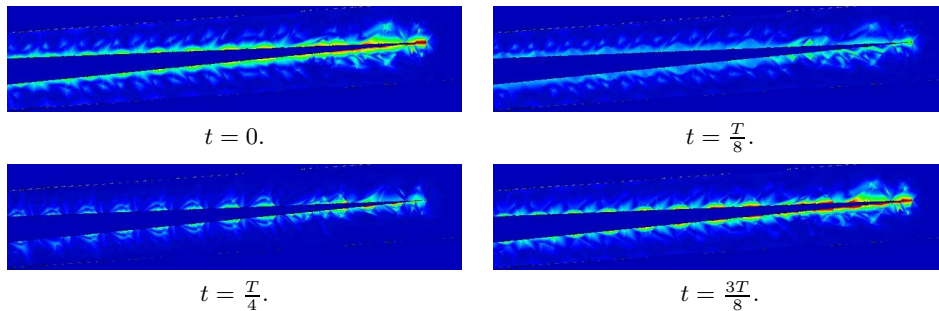


$f = 12.5$  Hz

$f = 50$  Hz

$f = 200$  Hz

Figure 5: Absolute value of eddy currents for various frequencies.



$t = 0.$

$t = \frac{T}{8}.$

$t = \frac{T}{4}.$

$t = \frac{3T}{8}.$

Figure 6: Absolute value of eddy currents in the slitted tube, for various  $t$ .<sup>4</sup>

Figure 6 plots results for the welding problem and its changes over time. The figure shows the eddy currents in a plane that clips the slitted tube. Due to the extremely small penetration depth

<sup>4</sup> $T = \frac{1}{f}$  means the length of the period.

we present a zoom of the region close to the tip of the cut.

We point out that the numerical behavior is similar to the shielding problem. In Figure 6, the number of unknowns on the finest mesh equals  $n = 117814$  per Fourier coefficient. For this example, discretization was done by lowest order Nédélec elements of the second kind.

## 7 Concluding Remarks

In this paper we presented an efficient solver for three-dimensional nonlinear eddy current problems; instead of implementing a costly time-stepping scheme, we took advantage of the periodicity of the solution by applying a multiharmonic ansatz.

The efficiency of the multiharmonic approach in combination with multigrid techniques has been demonstrated by numerical computations for several problems.

Although one could see that the solver performs well, there is still room for improvement. One issue of further research might be, for example, the analysis and implementation of multigrid methods for non-symmetric problems, what would result in a considerable speed-up in the solution of the linearized systems.

Another very important topic is anisotropic meshing in the layer of strong induction in order to reduce the total amount of unknowns. Moreover, aiming at a further reduction of the problem size, one could consider a combination of local refinement with an increase of the polynomial degree of the finite element space.

## Acknowledgments

This work has been supported by the Austrian Science Fund “Fonds zur Förderung der wissenschaftlichen Forschung (FWF)” under the grants SFB F013, P 14953 and START Y192.

## References

- [1] D. N. Arnold, R. S. Falk, and R. Winther, *Multigrid in  $\mathbf{H}(\text{div})$  and  $\mathbf{H}(\text{curl})$* , Numer. Math. **85** (2000), 197–218.
- [2] F. Bachinger, *Multigrid Solvers for 3D Multiharmonic Nonlinear Magnetic Field Computations*, Diploma thesis, Institute for Computational Mathematics, Johannes Kepler University, Linz, 2003.
- [3] F. Bachinger, M. Kaltenbacher, and S. Reitzinger, *An Efficient Solution Strategy for the HBE Method*, Proceedings of the IGTE '02 Symposium Graz, Austria, 2002, pp. 385–389.
- [4] F. Bachinger, U. Langer, and J. Schöberl, *Numerical Analysis of Nonlinear Multiharmonic Eddy Current Problems*, SFB-Report No. 04-01, Johannes Kepler University Linz, SFB “Numerical and Symbolic Scientific Computing”, 2004.
- [5] R. Beck, R. Hiptmair, R. H. W. Hoppe, and B. Wohlmuth, *Residual based a posteriori error estimators for eddy current computations*, M2AN Math. Model. Numer. Anal. **34** (2000), 159–182.
- [6] R. W. Freund and N. M. Nachtigal, *QMR: a quasi-minimal residual method for non-Hermitian linear systems*, Numer. Math. **60** (1991), 315–339.
- [7] H. de Gersem, H. V. Sande, and K. Hameyer, *Strong coupled multiharmonic finite element simulation package*, COMPEL **20** (2001), 535–546.
- [8] J. Gyselinck, P. Dular, C. Geuzaine, and W. Legros, *Harmonic-Balance Finite-Element Modeling of Electromagnetic Devices: A Novel Approach*, IEEE Transactions on Magnetics **38** (2002), 521–524.

- [9] W. Hackbusch, *Multi-grid Methods and Applications*, Springer, Berlin, 2003.
- [10] B. Heise, *Analysis of a Fully Discrete Finite Element Method for a Nonlinear Magnetic Field Problem*, SIAM J. Numer. Anal. **31** (1994), no. 3, 745–759.
- [11] R. Hiptmair, *Multigrid method for Maxwell's equations*, SIAM J. Numer. Anal. **36** (1999), 204–225.
- [12] R. Hiptmair, *Finite elements in computational electromagnetism*, Acta Numerica (2002), 237–339.
- [13] N. Ida and P. A. Bastos, *Electromagnetics and Calculation of Fields*, Springer, New York, 1997.
- [14] M. Kuhn, U. Langer, and J. Schöberl, *Scientific Computing Tool for 3D Magnetic Field Problems*, The Mathematics of Finite Elements and Applications: Highlights 1999, MAFELAP 1999 (J.R. Whiteman, ed.), John Wiley & Sons, Ltd., 2000, pp. 239–258.
- [15] P. Monk, *Finite Element Methods for Maxwell's Equations*, Numerical Mathematics and Scientific Computation, Oxford Science Publications, Clarendon Press, Oxford, 2003.
- [16] J. C. Nédélec, *Mixed Finite Elements in  $\mathbb{R}^3$* , Numer. Math. **93** (1980), 315–341.
- [17] ———, *A New Family of Mixed Finite Elements in  $\mathbb{R}^3$* , Numer. Math. **50** (1986), 57–81.
- [18] G. Paoli, O. Bíró, and G. Buchgraber, *Complex representation in nonlinear time harmonic eddy current problems*, IEEE Transactions on Magnetics **34** (1998), 2625–2628.
- [19] C. Pechstein, *Multigrid-Newton-Methods for Nonlinear Magnetostatic Problems*, Diploma thesis, Institute of Computational Mathematics, Johannes Kepler University, Linz, 2004.
- [20] S. Reitzinger, B. Kaltenbacher, and M. Kaltenbacher, *A Note on the Approximation of B-H Curves for Nonlinear Magnetic Field Computations*, SFB-Report No. 02-30, Johannes Kepler University Linz, SFB “Numerical and Symbolic Scientific Computing”, 2002.
- [21] J. Schöberl, *NGSolve - 3D Finite Element Solver*, <http://www.hpfem.jku.at/ngsolve/>.
- [22] ———, *NETGEN - An advancing front 2D/3D-mesh generator based on abstract rules*, Comput. Visual. Sci. **1** (1997), 41–52.
- [23] R. Verfürth, *A Review of A Posteriori Error Estimation and Adaptive Mesh-Refinement Techniques*, Wiley-Teubner, Chichester, 1996.
- [24] S. Yamada and K. Bessho, *Harmonic field calculation by the combination of finite element analysis and harmonic balance method*, IEEE Transactions on Magnetics **24** (1988), 2588–2590.
- [25] J. Z. Zhu and O. C. Zinkiewicz, *Adaptive techniques in the finite element method*, Commun. Appl. Numer. Methods **4** (1988), 197–204.
- [26] O. C. Zinkiewicz and J. Z. Zhu, *A simple error estimator for practical engineering analysis*, Int. J. Numer. Meth. Engg. **24** (1987), 337–357.